ISSN: 1999-6691, e-ISSN: 2782-3709 DOI: 10.7242/1999-6691/2026.19.1.1

Research article

Numerical modeling of diurnal oscillation of insolation in the idealized model of general atmospheric circulation

A.A. Gavrilov[1]***, A.N. Sukhanovskii***[2]

[1] *Kutateladze Institute of Thermophysics SB RAS, Novosibirsk, Russian Federation*
[2] *Institute of Continuous Media Mechanics UB RAS, Perm, Russian Federation*

The Earth's rotation around its axis causes the sunlit region to constantly shift in the opposite direction. The resulting diurnal oscillations of the surface temperature can influence the structure and dynamics of the general circulation and midlatitude baroclinic waves. This paper presents a numerical study of the influence of diurnal insolation oscillations on the formation and characteristics of large-scale flows using a numerical twin of the laboratory model of atmospheric general circulation. Two main regimes were considered: with regular and irregular baroclinic waves. Diurnal insolation oscillations were modeled using a localized, moving heat source. It is shown that for both regimes of baroclinic waves, the transition from stationary, zonally uniform heating to non-stationary, zonally inhomogeneous heating does not lead to qualitative changes of the mean flow structure or the distribution of pulsations. This only leads to quantitative changes, the magnitude of which does not exceed 15%. The hypothesis that a moving heat source would lead to an increase in pulsation energy was not confirmed. Moreover, the energy of meridional velocity pulsations, which characterizes the energy of baroclinic waves, decreases in the case of a moving heat source. A relatively weak effect of the transition from a stationary, zonally uniform heating regime to a non-stationary, localized one is explained by the fact that disturbances caused by the movement of the heat source are both spatially and frequency-localized.

Keywords: rotating convection, localized heating, general atmospheric circulation, baroclinic waves

Received: 25.11.2025 / *Published online*: 25.02.2026

1. Introduction

The general circulation of the atmosphere (GCA) governs the transport of heat between low and high latitudes, thereby playing a crucial role in weather and regional climate. [1]. The characteristics and temporal evolution of the GCA depend on a wide range of factors, including Earth's rotation, solar radiation, surface topography, and many others. Accounting for these factors is essential for weather prediction; however, as a result, the mathematical models employed for this purpose are extremely complex [2–4]. The large number of parameters and tunable settings in models describing hydrodynamic and thermodynamic processes significantly complicates their use (in their full formulation) for identifying the mechanisms responsible for the formation of large-scale zonal and meridional flows and waves of various origins [5, 6]. For this purpose, simplified models with varying degrees of idealization are employed [7, 8]. The evident similarity between the mean structure of the GCA and the distribution of wave activity in reanalysis data [9], idealized full-scale models [10–12], and laboratory models [13–15] makes it possible, at least as a first approximation, to model the GCA using a rotating convective layer with a meridional temperature difference within a certain range of control parameters. As an example of the successful application of an idealized laboratory model, one can note the identification of mechanisms of Arctic amplification of the warming. Changes in temperature distribution, the intensity of zonal flows, and baroclinic waves in experiments and numerical simulations carried out within the framework of a laboratory GCA model in [15] are in good qualitative agreement with results obtained using climate models [16, 17] and reanalysis data [18]. At the same time, the relative simplicity and limited number of parameters of the laboratory GCA model allowed us to identify, among the possible mechanisms responsible for

©Authors 2026 Translation of the original article in Russian This is an open access article under the CC BY 4.0 license

enhanced Arctic warming, a mechanism based on the weakening and displacement of the polar meridional cell. In [19], the transformation of the GCA and the mean and fluctuating components of meridional heat transport were studied as functions of rotation rate. The key results of [19], such as the dependence of the number of meridional cells on the rotation rate, are also in good agreement with full-scale aquaplanet simulations [10].

Seasonal oscillations of insolation can significantly affect the characteristics of the GCA and baroclinic waves [11, 12]. In addition to relatively slow seasonal variations, insolation is characterized by rapid diurnal oscillations. The heat source (the region illuminated by the Sun) moves over the Earth's surface in the direction opposite to its rotation. It is well known that diurnal variations strongly influence phase transitions, moisture content [20, 21], wind intensity [22], and convection [23]. The influence of diurnal oscillations on the modulation of Rossby wave amplitudes at low latitudes has also been suggested [24]. A review of the literature indicates that the important question of how diurnal oscillations affect the formation and dynamics of large-scale atmospheric flows has not received sufficient attention and remains open. It should be noted that the formation of convective flows in the presence of a heat source moving in the zonal direction has been studied in a number of works (including recent studies), but only for a non-rotating layer. Initially, the question addressed was whether zonal circulation could develop in a stationary cylindrical layer in the presence of a heat source rotating in the laboratory frame. Experiments [25, 26] demonstrated that zonal flows do indeed form, and in the direction opposite to the rotation of the heat source. Numerical simulations [27] have shown that, depending on the parameters (angular velocity of the heat source and heating intensity), zonal flows can either lag behind or lead the source.

In the present work, the influence of diurnal insolation oscillations on the formation and characteristics of large-scale flows is investigated using a numerical twin of the laboratory GCA model.

2. Methods

The study is based on a digital twin of the laboratory GCA model. A detailed description of the laboratory model, as well as a comparison of laboratory and numerical results, can be found in [13, 15, 19]. A scheme of the computational domain is shown in Fig. 1*a*. The working volume is a cylindrical fluid layer with a free surface, having a radius $R = 345$ mm and a height $h = 30$ mm. An annular heater of width 25 mm is located at the bottom boundary. The distance from the lateral cylindrical wall to the outer boundary of the heater is 40 mm. Silicone oil PMS-5 is used as the working fluid.

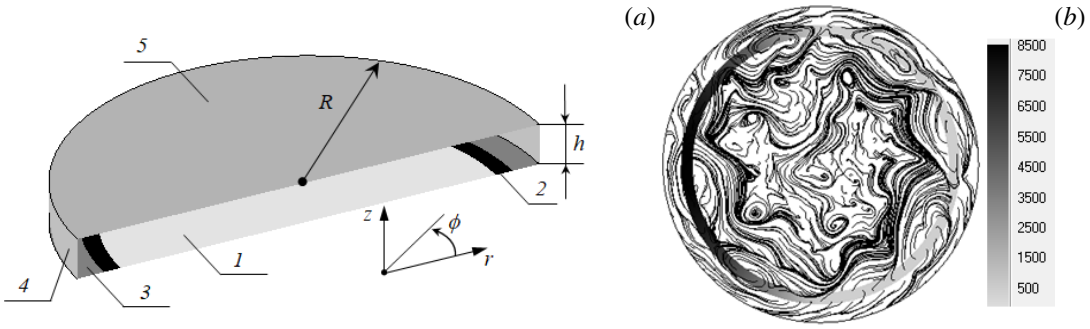


Fig. 1. Scheme of the computational domain: *1*, *3*, *4* – rotating adiabatic walls, no-slip condition; *2* – annular heater; *5* – free surface (heat exchange with air), slip condition (*a*); temperature distribution T [K] in the region of the moving annular heater (shown by color) and an example of instantaneous flow near the free surface (streamlines) (*b*)

The unsteady flow of an incompressible fluid is modeled within the Boussinesq approximation in a rotating reference frame by the following equations:

$$\nabla \cdot \mathbf{u} = 0,$$

$$\frac{\partial \mathbf{u}}{\partial t}+(\mathbf{u}\cdot\nabla)\mathbf{u}+(2\boldsymbol{\Omega}\times\mathbf{u}+\boldsymbol{\Omega}\times\boldsymbol{\Omega}\times\mathbf{r})=-\frac{\nabla p}{\rho}+\nu\nabla^2\mathbf{u}-\beta(T-T_0)g,$$

$$\frac{\partial T}{\partial t}+(\mathbf{u}\cdot\nabla)T=\chi\nabla^2 T,$$

where $\mathbf{u}$ is the relative velocity vector (hereafter referred to as velocity), $\boldsymbol{\Omega}$ is the angular velocity vector of the system rotation about the central axis, $\mathbf{r}$ is the local radius vector, p is pressure, ρ is density, ν is kinematic viscosity, β is the thermal expansion coefficient, T is temperature, T_0 is a reference temperature, g is gravitational acceleration, and χ is thermal diffusivity.

No-slip boundary conditions are imposed on all solid walls, while a slip condition is applied at the free surface. The thermal regime is determined by the power of the heater and the cooler. For the basic heat transfer case, the powers of the heater and the cooler (free surface) are $Q_h = 123$ W. A heat flux is specified on the heater and the cooler, calculated based on their rated thermal power and surface area. All other solid surfaces are adiabatic.

In a series of simulations, a localized heat source is modeled at the periphery, in the region of the annular heater, moving in the rotating reference frame opposite to the rotation of the layer with angular velocity Ω (Fig. 1*b*). The rotating localized heat source mimics solar illumination. The heat flux density from the localized source is calculated as follows:

$$q(\phi,t)=\frac{\pi Q_{local}}{A_h}\max[0,\sin(\phi+\Omega t)],$$

where Q_{local} is the thermal power of the localized source, A_h is the area of the annular heater, and ϕ is the local azimuthal angle.

Two regimes are considered: with regular and irregular baroclinic waves [13, 19]. The corresponding angular velocities are 0.23 and 0.37 rad/s. As dimensionless parameters characterizing rotational effects, the Ekman number and the Taylor number are typically used:

$$\mathrm{Ek}=\nu/(\Omega h^2),$$

$$\mathrm{Ta}=4\Omega^2 R^5/(h\nu^2).$$

For the regime with regular waves, the control parameters are $\mathrm{Ek}=0.025$, $\mathrm{Ta}=1.4\cdot10^9$, while for the regime with irregular waves they are $\mathrm{Ek}=0.015$, $\mathrm{Ta}=3.6\cdot10^9$. The Ekman number characterizes the thickness of the viscous boundary layer near the bottom boundary of the model. In the considered regimes, this thickness is on the order of 4 mm. For each regime, three heating configurations are considered: azimuthally uniform heating, a moving localized heat source, and combined heating including both azimuthally uniform heating and a moving localized heat source. The total heating power is fixed and equal to 123 W for all configurations. Heating and cooling are balanced such that the total heat flux across all boundaries is zero, and the volume-averaged temperature remains constant.

The initial approximation for the fluid velocity corresponds to solid-body rotation. The initial temperature is assumed to be uniform and equal to 20° C.

Discretization. An unstructured computational mesh is employed, consisting of several blocks with structured hexahedral cells. The blocks define the regions of the heater and the localized cooler. In the cooler region, a five-block structured mesh with a central square is used. The square is covered by a uniform structured mesh. In the vertical direction, the mesh is refined toward the upper and lower boundaries of the computational domain and contains N_z nodes. Approximately, the base computational mesh has the following resolution: 192 nodes in the radial direction with refinement toward the heater and cooler, 260 nodes in the tangential direction, and 40 nodes in the vertical direction with a refinement factor of 1.05 toward the model boundaries. The total number of control volumes is 2.0 million.

The time integration step is 0.1 s and remains constant throughout the simulation. For the baseline regime

with a rotation period of 17 s, the maximum Courant–Friedrichs–Lewy (CFL) number, computed based on the relative velocity, does not exceed 3.0, while the volume-averaged value is $\mathrm{CFL} = 0.2 \pm 0.2$. Statistical characteristics are obtained by averaging over time and the azimuthal direction after reaching a statistically steady state. The transient phase lasts about 2000 s. The averaging time is at least 7200 s.

Numerical algorithm. Numerical simulations are performed using the SigmaFlow package; the numerical algorithm is based on the finite volume method for spatial discretization of the governing hydrodynamic equations on an unstructured mesh. The convective and diffusive terms in the momentum equation are approximated using second-order central difference schemes. The coupling between velocity and pressure fields, ensuring satisfaction of the continuity equation, is implemented using a SIMPLE-type splitting procedure. The velocity and pressure fields are defined at the centers of control volumes. To suppress pressure oscillations, the Rhie–Chow approach is applied, which involves a special interpolation of the velocity vector at the faces of control volumes. Time integration of the momentum equation is performed using the second-order Crank–Nicolson method, with both viscous and convective terms treated implicitly. The convective terms in the energy equation are approximated using an upwind TVD scheme, while the unsteady term in the temperature equation is approximated using a three-level second-order scheme. The pressure correction is obtained from the corresponding discrete equation using an algebraic multigrid method. Parallel computing technology based on domain decomposition into multiple adjacent subdomains is employed to accelerate the computations.

Verification and validation. Verification of the numerical model was previously performed by the authors; see [15].

3. Results

The influence of a moving extended heat source on the flow characteristics in the laboratory GCA model was studied in two regimes: quasi-regular and irregular baroclinic waves. The structure of the mean and instantaneous flows in the latter regime most closely resembles that observed in the real atmosphere [15]; therefore, for brevity, hereafter we refer to this regime as the atmospheric one. This makes it possible to assess the influence of diurnal temperature oscillations for different wave regimes. The regime with stationary heating, described in detail in [15], is used as the basic case. We restrict ourselves to a brief description of the main features required for the comparative analysis. The mean and fluctuating flow characteristics for the basic state, i.e., stationary heating, are shown in Figs. 2, 3*a*, and 4*a*. The mean meridional circulation consists of analogues of the three main atmospheric cells (Fig. 2*a*). The most intense is the analogue of the Hadley cell located near the heating region; at smaller radii there is an analogue of the midlatitude cell (the Ferrel cell), and finally, near the rotation axis, an analogue of the polar cell is formed. Because the heating region is displaced from the sidewall, one more (additional) cell arises near it; this cell is not of interest in the present study. The structure of the zonal flows (in the rotating frame of reference) is also qualitatively similar to the structure of flows observed in the atmosphere (Fig. 2*b*). At the periphery, a flow directed opposite to the rotation of the layer (anticyclonic) is formed, which is an analogue of the easterlies. At smaller radii, an analogue of the westerlies appears, namely a flow co-directed with the rotation of the layer (cyclonic). The velocity of the zonal flows V in the GCA model, as in the real atmosphere, increases with height z.

The mean temperature distribution is shown in Fig. 3*a*. A characteristic feature of convection in a rotating layer is the inclination of the isotherms. At the same time, almost everywhere, except for the region adjacent to the heater, the temperature increases with height, i.e., stable stratification is formed. Fluctuations of the meridional velocity are primarily associated with baroclinic waves and are commonly used as an indicator of wave activity (Fig. 4*a*). Baroclinic waves form in the region with the strongest horizontal temperature gradient, which is shifted away from the heating region toward smaller radii (Fig. 3*a*). The maximum wave activity is located in the upper part of the layer, just as in the real atmosphere, where the highest level of meridional velocity fluctuations is observed in the upper troposphere. Temperature fluctuations shown in Fig. 4*b* are also caused by baroclinic waves. A high level of temperature fluctuations characterizes the region of baroclinic waves and the strongest heat flux.

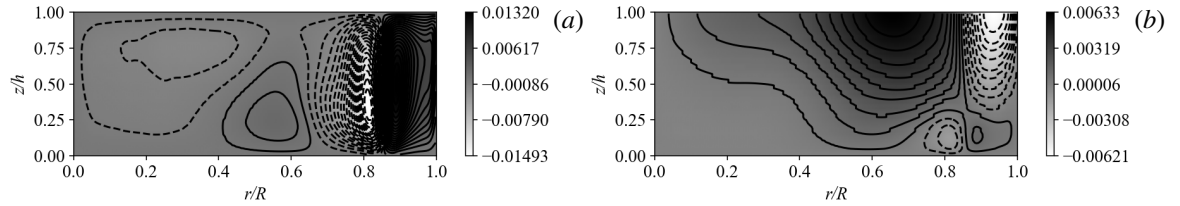


Fig. 2. Mean meridional circulation (streamfunction distribution [m^2/s]) (*a*) and distribution of the mean zonal flows [m/s] (*b*) in the atmospheric regime; dashed lines denote isolines with negative values, and solid lines denote isolines with positive values

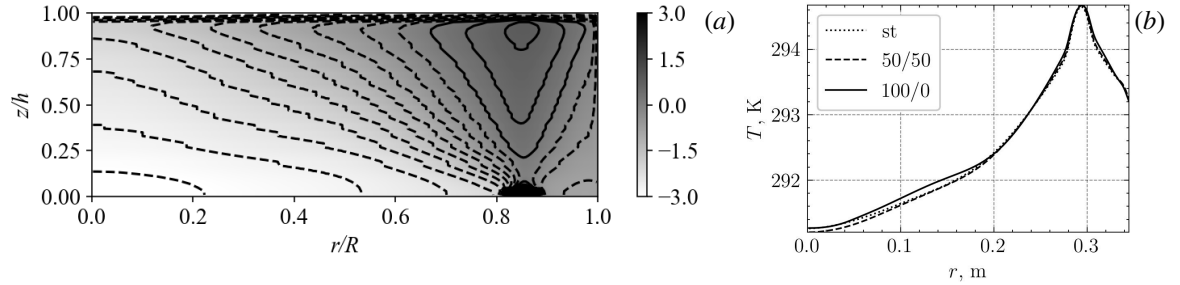


Fig. 3. Mean (time- and zonal-coordinate-averaged) temperature distribution ($T - T_0$) [K] for stationary heating (*a*); mean (time-, zonal-coordinate-, and height-averaged) radial temperature profiles for different heating configurations (*b*): st – stationary, 50/50 – combination of stationary heating and moving source, 100/0 – moving source; atmospheric regime

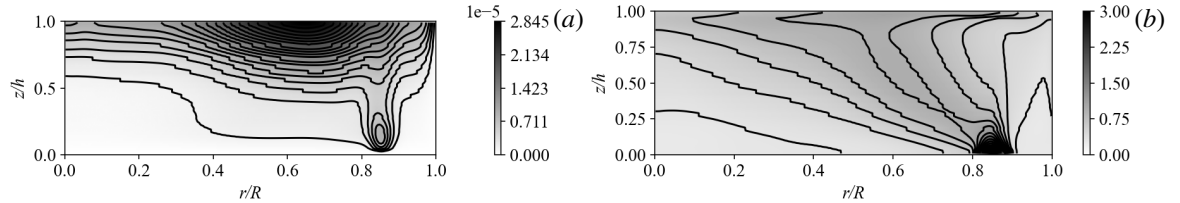


Fig. 4. Distributions of velocity fluctuation energy [m^2/s^2] (*a*) and temperature fluctuation energy [K^2] (*b*); atmospheric regime, stationary heating

Let us consider the changes in the mean and fluctuating flow characteristics in the presence of a heat source moving opposite to the direction of rotation. Figure 3*b* shows that the mean temperature distribution depends only weakly on the heating configuration. The radial temperature profiles (averaged over time, zonal coordinate, and height) for the stationary zonally symmetric heater and the moving localized heater practically coincide. In contrast to the temperature profiles, the transition to another heating configuration leads to quantitative changes in the mean zonal flows that depend strongly on the system rotation rate, while their overall structure is preserved. In the regime of quasi-regular baroclinic waves, the transition from zonally uniform stationary heating to a moving source is accompanied by a weakening of the zonal flow (the analogue of the westerlies) (Fig. 5*a*, *b*), whereas in the atmospheric regime, by contrast, the main zonal flow becomes stronger and is displaced toward the periphery (Fig. 5*c*, *d*). However, the described changes are relatively small and do not affect the flow structure as a whole.

The results concerning the fluctuating characteristics turned out to be unexpected. The moving localized heater is itself a source of disturbances; therefore, one could expect its presence to lead to a substantial increase in the level of velocity fluctuations. However, as the simulation results show, this is not the case. The mean (height- and zonal-coordinate-averaged) profiles of the velocity fluctuation energy for the three heating configurations and the two different flow regimes are shown in Fig. 6. It is clearly seen that the level of fluctuations in the region of baroclinic waves at intermediate radii of the fluid layer decreases in the case of a localized heat source in both regimes. At the same time, as in the mean flow, no qualitative changes occur in

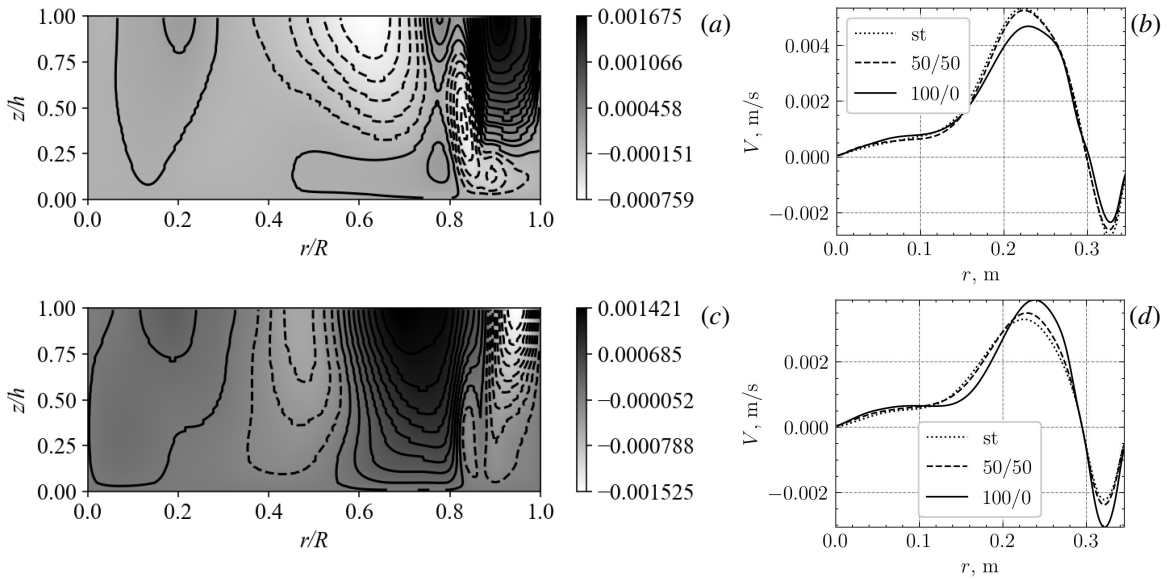


Fig. 5. Changes in the distribution of zonal flows [m/s] in the case of a moving heat source (*a*, *c*), mean (height-, zonal-coordinate-, and time-averaged) profiles of zonal velocity for three heating configurations (*b*, *d*); regime of quasi-regular baroclinic waves (*a*, *b*), atmospheric regime (*c*, *d*)

the distribution of fluctuations. However, this does not mean that the transition to another heating configuration does not affect the instantaneous characteristics of baroclinic waves.

A common approach for illustrating the evolution of baroclinic waves is to use temporal dependencies of meridional velocity fluctuation profiles (Hovmöller diagrams). Recall that baroclinic waves are move with the zonal flow and move in the rotating frame of reference in the direction of rotation. Figure 7 presents the profiles of meridional velocity fluctuations at the upper boundary of the layer, along a fixed radial direction in the time–radius plane, for the two wave regimes considered and the two heating configurations at the periphery. The qualitative changes in the characteristics of baroclinic waves during the transition from the quasi-regular (Fig. 7*a, b*) to the atmospheric (Fig. 7*c*, *d*) regime are clearly visible, which cannot be said about the influence of the heating configuration. Here, as previously for the mean characteristics, some noticeable but non-fundamental changes can be seen. Thus, for quasi-regular waves, the transition to a moving heat source leads to a decrease in the phase velocity of the waves and an increase in their meridional size. High-frequency fluctuations at the periphery caused by the motion of the heat source are also noticeable (Fig. 7*b*). Changes

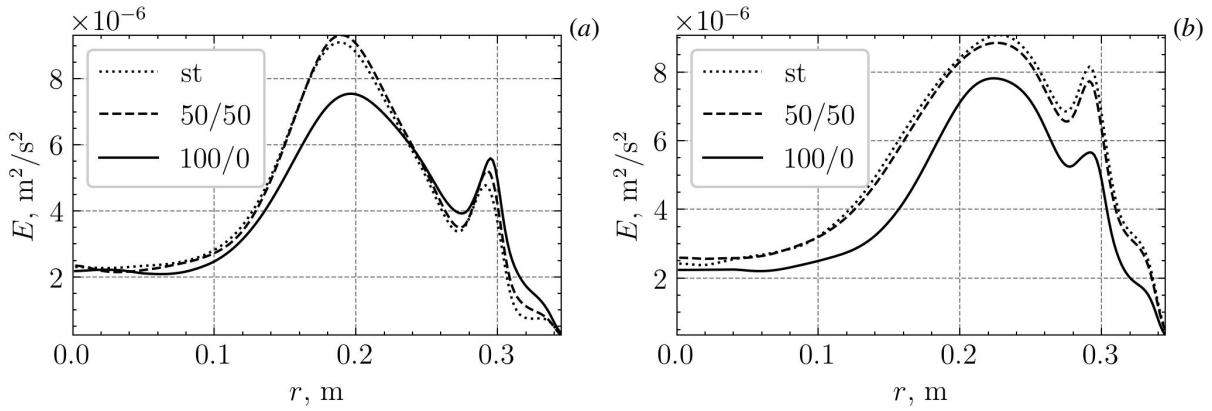


Fig. 6. Mean (height- and zonal-coordinate-averaged) profiles of the meridional velocity fluctuation energy for three heating configurations in the regime of quasi-regular baroclinic waves (*a*) and in the atmospheric regime (*b*)

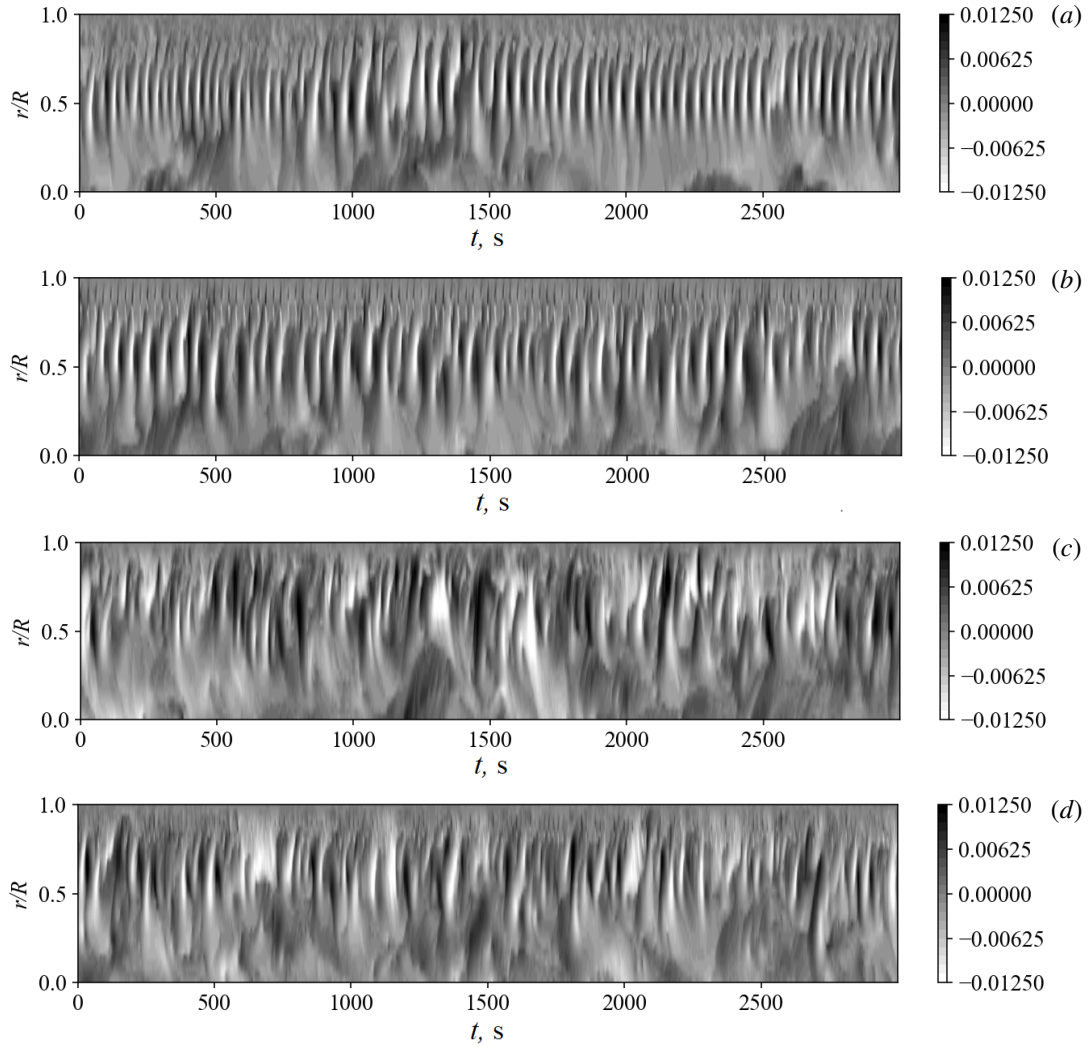


Fig. 7. Hovmöller diagrams of meridional velocity fluctuations [m/s] at the upper boundary of the layer for a fixed azimuthal angle ϕ in the "time–radius" plane for different flow regimes and heating configurations: regime of quasi-regular baroclinic waves (*a*, *b*); atmospheric regime (*c*, *d*); stationary heating (*a*, *c*); moving localized source (*b*, *d*)

in the character of baroclinic waves in the atmospheric regime are even less pronounced. The Hovmöller diagrams for azimuthal profiles (Fig. 8) illustrate the features of baroclinic waves for the two regimes and show that a relatively small variation in angular velocity fundamentally affects the wave dynamics. The minima and maxima in Fig. 8 correspond to individual wave structures (vortices). The length and slope of the lines, clearly distinguishable for the regular-wave regime (Fig. 8*a*, *b*), characterize the lifetime of individual vortices and their phase velocity. In the atmospheric regime (Fig. 8*c*, *d*), the wave motion is more complex. It should also be noted that, in contrast to the regular regime, the wave lifetime in the atmospheric regime is substantially limited: the waves break down before completing a full revolution. At the same time, even in the regime with regular waves, noticeable rearrangements of the wave structure are possible, accompanied by changes in the wave number (the number of vortices) and in the wave amplitude. As for the main question, namely the influence of changes in the heating configuration on wave formation, it is difficult to give an unambiguous answer. Qualitative analysis does not reveal any substantial differences between the results for zonally uniform heating and heating by a moving source; that is, in general, the overall pattern of wave motion does not depend on the heating configuration.

The energy spectra of meridional velocity fluctuations, which characterize the energy of baroclinic waves,

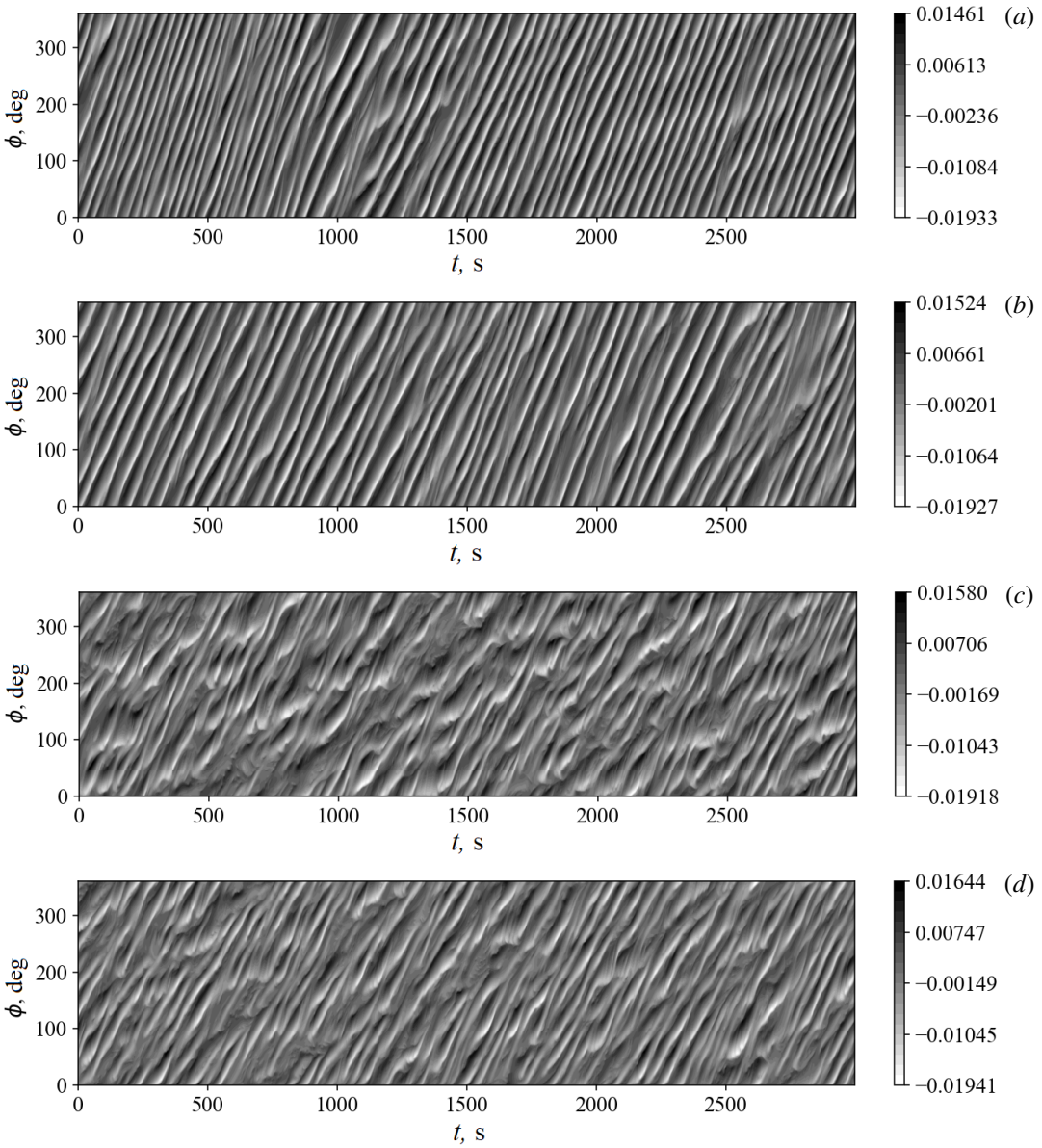


Fig. 8. Hovmöller diagrams of meridional velocity fluctuations [m/s] at the upper boundary of the layer for $r/R \approx 0.53$ in the "time–azimuthal angle" plane: regime of quasi-regular baroclinic waves (*a*, *b*), atmospheric regime (*c*, *d*), stationary heating (*a*, *c*), moving localized source (*b*, *d*)

are shown in Fig. 9 for different regimes and heating types. The spectra are constructed using the decomposition of meridional velocity fluctuations into azimuthal Fourier modes [11–13] over the entire statistically stationary time interval. The spectra for both regimes show a decrease in the fluctuation level in the case of a moving heat source. In the quasi-regular regime, the energy maximum shifts toward lower (larger-scale) spatial modes, whereas in the atmospheric regime, by contrast, it shifts toward higher modes. In Figs. 7 and 8, one can note an increase in the size of the structures characterizing baroclinic waves in the quasi-regular regime and their decrease in the atmospheric regime in the case of a moving heat source. The relatively weak effect of changing the heating regime from stationary zonally uniform to unsteady localized heating is explained by the fact that the disturbances induced by the motion of the heat source are localized both in space and in frequency. This is clearly seen in the distributions of fluctuation energy in the radius–wave mode plane (Fig. 10) and the radius–frequency plane (Fig. 11). The distribution of localized heating is characterized by the lowest mode

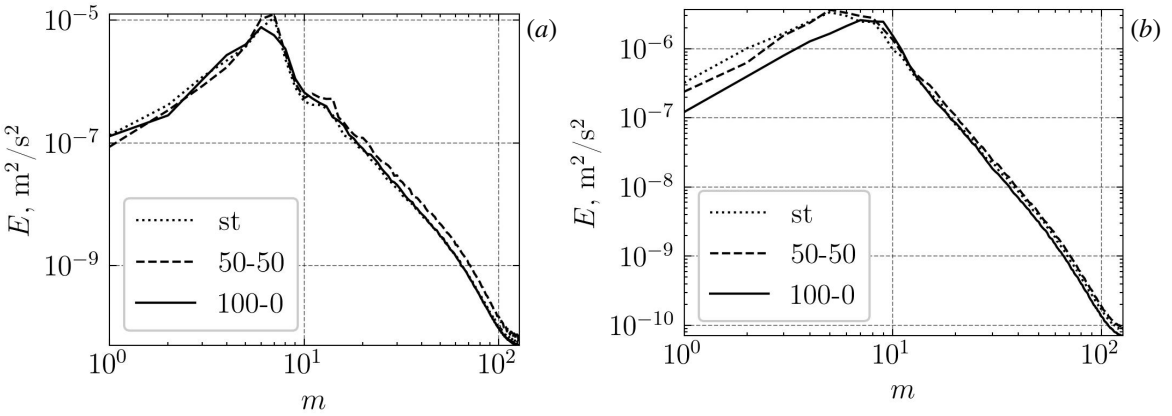


Fig. 9. Energy spectra of meridional velocity fluctuations [m^2/s^2] for the quasi-regular (*a*) and atmospheric (*b*) regimes for different heating configurations

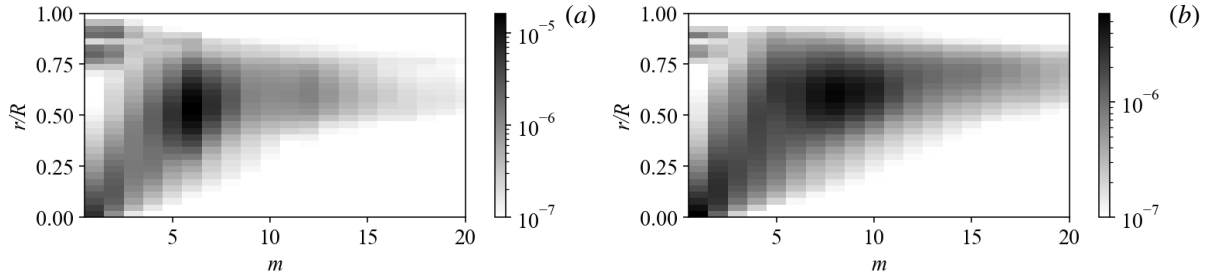


Fig. 10. Distribution of the meridional velocity fluctuation energy [m^2/s^2] in the "radius–wave mode" plane for different flow regimes: quasi-regular (*a*), atmospheric (*b*)

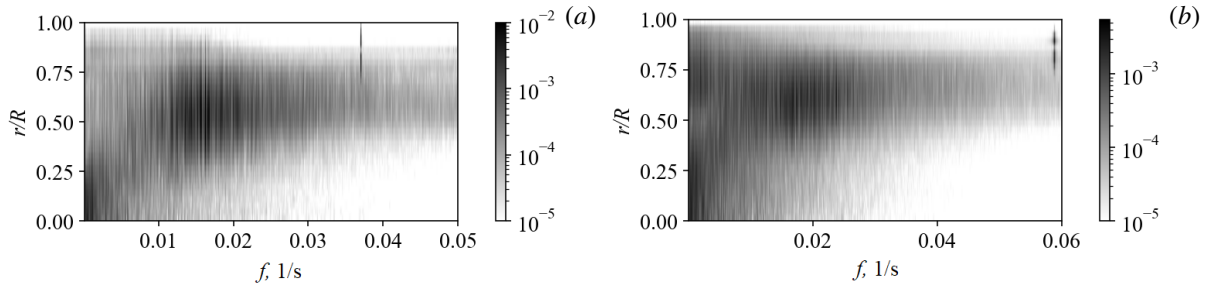


Fig. 11. Distribution of the meridional velocity fluctuation energy [m^2/s^2] in the "radius–frequency" plane: quasi-regular regime (*a*), atmospheric regime (*b*)

$m = 1$; therefore, one may expect that the motion of the heat source will generate large-scale modes. Indeed, this is clearly seen in Fig. 10: the velocity fluctuations caused by the motion of the heat source are described by the lowest spatial modes ($m = 1$ and $m = 2$), which are located at the periphery and practically do not penetrate into the region of baroclinic waves. The frequency distribution of fluctuations (Fig. 11) shows that the forcing frequency associated with the motion of the heat source is significantly higher than the frequencies characteristic of baroclinic waves, especially in the atmospheric regime.

4. Conclusion

A numerical study of the influence of diurnal insolation oscillations on the formation and characteristics of large-scale flows has been carried out using a numerical twin of the laboratory GCA model. The results turned out to be unexpected. In particular, the transition from stationary zonally uniform heating to heating

by a moving heat source, which models diurnal insolation oscillations, did not lead to qualitative changes in the characteristics of the mean flow or in the distribution of fluctuations. Only quantitative changes in the velocity of the main zonal flow (the analogue of the westerlies) and in meridional velocity fluctuations were observed. It is shown that the mean temperature distribution is practically independent of the heating configuration. It is worth noting that heating by a moving heat source affects the main zonal circulation differently in various baroclinic-wave regimes: in the quasi-regular regime the zonal flow weakens, whereas in the atmospheric regime it strengthens. However, the magnitude of these deviations from the basic case (zonally uniform heating) does not exceed 15%. The assumption that a moving heat source would generate additional disturbances and, consequently, increase the fluctuation energy was not confirmed. On the contrary, the energy of meridional velocity fluctuations, which characterizes the energy of baroclinic waves, decreases in the presence of a moving heat source. The relatively weak effect of changing the heating regime (from stationary zonally uniform to unsteady localized) is explained by the fact that the disturbances induced by the motion of the heat source are both spatially and frequency-localized. The lowest spatial modes are located at the periphery and practically do not penetrate into the region of baroclinic wave formation, while the forcing frequency associated with the motion of the heat source is significantly higher than the frequencies characterizing baroclinic waves.

The research was supported by the Russian Science Foundation (project No. 22-61-00098).

References

1. *Vallis G.K.* Atmospheric and oceanic fluid dynamics. Cambridge University Press, 2017
2. *Volodin E.M.*, *Mortikov E.V.*, *Kostrykin S.V.*, *Galin V.Y.*, *Lykosov V.N.*, *Gritsun A.S.*, *Dianskii N.A.*, *Gusev A.V.*, *Yakovlev N.G.* Simulation of Modern Climate with the New Version of the INM RAS Climate Model. Izvestiya Atmospheric and Oceanic Physics. 2017. Vol. 53, no. 2. P. 164–178. DOI: 10.7868/S0002351517020122
3. *Majumdar S.J.*, *Sun J.*, *Golding B.*, *et al.* Multiscale Forecasting of High-Impact Weather: Current Status and Future Challenges. Bulletin of the American Meteorological Society. 2021. Vol. 102, no. 3. P. E635–E659. DOI: 10.1175/BAMS-D-20-0111.1
4. *Brotzge J.A.*, *Berchoff D.*, *Carlis D.L.*, *Carr F.H.*, *Carr R.H.*, *Gerth J.J.*, *Gross B.D.*, *Hamill T.M.*, *Haupt S.E.*, *Jacobs N.*, *et al.* Challenges and opportunities in numerical weather prediction. Bulletin of the American Meteorological Society. 2023. Vol. 104, no. 3. P. E698–E705. DOI: 0.1175/BAMS-D-22-0172.1
5. *Vallis G.K.* Geophysical fluid dynamics: whence, whither and why?. Proceedings of the Royal Society A: Mathematical, Physical and Engineering Sciences. 2016. Vol. 472, no. 2192. 20160140. DOI: 10.1098/rspa.2016.0140
6. *Claussen M.*, *Mysak L.*, *Weaver A.*, *Crucifix M.*, *Fichefet T.*, *Loutre M.-F.*, *Weber S.*, *Alcamo J.*, *Alexeev V.*, *Berger A.*, *et al.* Earth system models of intermediate complexity: closing the gap in the spectrum of climate system models. Climate dynamics. 2002. Vol. 18. P. 579–586. DOI: 0.1007/s00382-001-0200-1
7. *Jeevanjee N.*, *Hassanzadeh P.*, *Hill S.*, *Sheshadri A.* A perspective on climate model hierarchies. Journal of Advances in Modeling Earth Systems. 2017. Vol. 9, no. 4. P. 1760–1771. DOI: 10.1002/2017MS001038
8. *Maher P.*, *Gerber E.P.*, *Medeiros B.*, *Merlis T.M.*, *Sherwood S.*, *Sheshadri A.*, *Sobel A.H.*, *Vallis G.K.*, *Voigt A.*, *Zurita-Gotor P.* Model Hierarchies for Understanding Atmospheric Circulation. Reviews of Geophysics. 2019. Vol. 57, no. 2. P. 250–280. DOI: 10.1029/2018RG000607
9. *Kalnay E.*, *Kanamitsu M.*, *Kistler R.*, *et al.* The NCEP/NCAR 40-Year Reanalysis Project. Renewable Energy. Routledge, 2018. P. 146–194. DOI: 10.4324/9781315793245-16
10. *Kaspi Y.*, *Showman A.P.* Atmospheric dynamics of terrestrial exoplanets over a wide range of orbital and atmospheric parameters. The Astrophysical Journal. 2015. Vol. 804, no. 1. P. 60. DOI: 10.1088/0004-637X/804/1/60
11. *Sukhanovskii A.*, *Stepanov R.*, *Bykov A.*, *Vetrov A.*, *Kalinin N.*, *Frick P.* Mid-latitude baroclinic waves in a zonally homogeneous Earth-like planet. Climate Dynamics. 2025. Vol. 63, no. 1. P. 1–21. DOI: 10.1007/s00382-024-07561-z

12. *Frick P.G.*, *Stepanov R.A.*, *Sukhanovskii A.N.*, *Kalinin N.A.*, *Vetrov A.L.*, *Bykov A.V.* General circulation and baroclinic Waves in the atmosphere of zonally uniform Earth-Like model planets. Izvestiya, Atmospheric and Oceanic Physics. 2025. Vol. 61, no. 6. P. 670–681.

13. *Sukhanovskii A.*, *Popova E.*, *Vasiliev A.* A shallow layer laboratory model of large-scale atmospheric circulation. Geophysical & Astrophysical Fluid Dynamics. 2023. P. 155–176. DOI: 10.1080/03091929.2023.2220877

14. *Vasiliev A.Y.*, *Popova E.N.*, *Sukhanovskii A.N.* The flow structure in a laboratory model of atmospheric general circulation. Computational Continuum Mechanics. 2023. Vol. 16, no. 3. P. 321–330. DOI: 10.7242/1999-6691/2023.16.3.27

15. *Sukhanovskii A.*, *Gavrilov A.*, *Popova E.*, *Vasiliev A.* The study of the impact of polar warming on global atmospheric circulation and mid-latitude baroclinic waves using a laboratory analog. Weather and Climate Dynamics. 2024. Vol. 5, no. 2. P. 863–880. DOI: 10.5194/wcd-5-863-2024

16. *Smith D.M.*, *Screen J.A.*, *Deser C.*, *et al.* The Polar Amplification Model Intercomparison Project (PAMIP) contribution to CMIP6: investigating the causes and consequences of polar amplification. Geoscientific Model Development. 2019. Vol. 12, no. 3. P. 1139–1164. DOI: 10.5194/gmd-2018-82

17. *Ye K.*, *Woollings T.*, *Sparrow S.N.*, *Watson P.A.G.*, *Screen J.A.* Response of winter climate and extreme weather to projected Arctic sea-ice loss in very large-ensemble climate model simulations. npj Climate and Atmospheric Science. 2024. Vol. 7, no. 1. P. 20. DOI: 10.1038/s41612-023-00562-5

18. *Blackport R.*, *Screen J.A.* Insignificant effect of Arctic amplification on the amplitude of midlatitude atmospheric waves. Science Advances. 2020. Vol. 6, no. 8. eaay2880. DOI: 10.1126/sciadv.aay2880

19. *Gavrilov A.*, *Sukhanovskii A.*, *Vasiliev A.*, *Popova E.* Numerical study of structural changes in the laboratory model of the atmospheric general circulation under variation of the rotation rate. International Journal of Heat and Mass Transfer. 2025. Vol. 241. 126676. DOI: 10.1016/j.ijheatmasstransfer.2025.126676

20. *Soden B.J.* The diurnal cycle of convection, clouds, and water vapor in the tropical upper troposphere. Geophysical Research Letters. 2000. Vol. 27, no. 15. P. 2173–2176. DOI: 10.1029/2000GL011436

21. *Lee M.-I.*, *Schubert S.D.*, *Suarez M.J.*, *Schemm J.-K.E.*, *Pan H.-L.*, *Han J.*, *Yoo S.-H.* Role of convection triggers in the simulation of the diurnal cycle of precipitation over the United States Great Plains in a general circulation model. Journal of Geophysical Research: Atmospheres. 2008. Vol. 113, no. D2. DOI: 10.1029/2007JD008984

22. *Dai A.*, *Deser C.* Diurnal and semidiurnal variations in global surface wind and divergence fields. Journal of Geophysical Research: Atmospheres. 1999. Vol. 104, no. D24. P. 31109–31125. DOI: 10.1029/1999JD900927

23. *Yang G.-Y.*, *Slingo J.* The Diurnal Cycle in the Tropics. Monthly Weather Review. 2001. Vol. 129, no. 4. P. 784–801. DOI: 10.1175/1520-0493(2001)129<0784:TDCITT>2.0.CO;2

24. *Raupp C.F.M.*, *Dias P.L.S.* Interaction of equatorial waves through resonance with the diurnal cycle of tropical heating. Tellus A: Dynamic Meteorology and Oceanography. 2010. Vol. 62, no. 5. P. 706–718. DOI: 10.1111/j.1600-0870.2010.00463.x

25. *Stern M.E.* The Moving Flame Experiment. Tellus A: Dynamic Meteorology and Oceanography. 1959. Vol. 11, no. 2. P. 175–179. DOI: 10.3402/tellusa.v11i2.9301

26. *Schubert G.*, *Whitehead J.A.* Moving Flame Experiment with Liquid Mercury: Possible Implications for the Venus Atmosphere. Science. 1969. Vol. 163, no. 3862. P. 71–72. DOI: 10.1126/science.163.3862.71

27. *Reiter P.*, *Zhang X.*, *Stepanov R.*, *Shishkina O.* Generation of zonal flows in convective systems by travelling thermal waves. Journal of Fluid Mechanics. 2021. Vol. 913. A13. DOI: 10.1017/jfm.2020.1186

Authors' Details:

Andrei Gavrilov, PhD; e-mail: gavand@yandex.ru; ORCID: 0009-0004-8061-0040

Andrei Sukhanovskii (corr.), D.SC., head of Dep., Institute of Continuous Media Mechanics, Perm; e-mail: san@icmm.ru; ORCID: 0000-0003-3178-0217